Journal of Porous Media 12(12), 1139–1152 (2009)

Analytical and Numerical Solution for One-Dimensional Two-Phase Flow in Homogeneous Porous Medium

Michal Beneš,[1]* Radek Fučík,[1] Jiří Mikyška,[1] and Tissa H. Illangasekare[2]

[1]Faculty of Nuclear Sciences and Physical Engineering, Czech Technical University in Prague, Trojanova 13, 120 00 Prague, Czech Republic

[2]Center for Experimental Study of Subsurface Environmental Processes, Colorado School of Mines, 1500 Illinois Street, 80401 Golden, Colorado, USA

*E-mail: benesm@kmlinux.fjfi.cvut.cz

ABSTRACT

The article presents a comparison of a semianalytical and a numerical approach to a one-dimensional flow-function model of two-phase flow through a homogeneous porous medium which is used for validation of more complex numerical models of two-phase flow. The flow-function model equation can be treated analytically to obtain an implicit formula for the saturation, which is resolved iteratively. This approach, originally derived by McWhorter and Sunada (1990; 1992), is used in its improved version so that we are able to readily obtain the wetting-phase saturation for all parameter values. To enlarge the class of admissible boundary and initial conditions, we propose another approach which relies on a numerical algorithm which solves the flow-function model equation, based on the finite-difference method in space and time, yielding values of the solution at given time moments and on a spatial grid of positions. Our approach is demonstrated in a series of one-dimensional computations showing the accuracy, efficiency, and generality of the proposed algorithms.

Received February 9, 2008; Accepted August 8, 2008

NOMENCLATURE

k_w, k_n, μ_w, μ_n, p_w, p_n	effective permeabilities, viscosities, and pressures (wetting and non-wetting phase)	$f(S_w)$, $D(S_w)$	flow function and diffusivity function
		Φ	porosity coefficient
q_t, q_w, q_n	total, wetting-phase and non-wetting phase volumetric flux	L, T	spatial dimension, length of the time interval
p_c, p_w, p_n	capillary, wetting-phase and non-wetting phase pressure	S_i, S_0	boundary and initial conditions for wetting-phase saturation
S_w, S_n	wetting-phase and non-wetting phasesaturation	S_{nr}	residual saturation of non-wetting phase

1. INTRODUCTION

Multidimensional complex numerical models of two-phase flow through porous medium such as the ones described in Helmig (1997), Mikyška et al. (2004), Mikyška and Illangasekare (2005), Beneš et al. (2006), and in Mikyška et al. (2009) require a thorough numerical testing, comparison, and validation to establish their reliability and usefulness. One of the tools for validation of such models is their comparison to analytical or semianalytical solutions of simplified models, namely, in one dimension. Among the results available for this task, one can use, e.g., the Buckley–Leverett solution of flow without capillary effects [e.g., described in Helmig (1997), or see references in McWhorter and Sunada (1990) and Fučík et al. (2005), and Fučík et al. (2007)]. An important tool widely used in the validation of models with capillary effects is described in McWhorter and Sunada (1990), with consequent discussions in Chen et al. (1992) and McWhorter and Sunada (1992). It allows an implicit functional equation for the wetting-phase saturation to be obtained, which has to be treated numerically to perform the functional inverse, yielding the saturation function of time and space. The procedure is established for the entry saturation limited by residual values. When using the entry saturation values near maximum under a particular parameter setting, we encounter difficulties in the numerical inversion. Another limitation of the McWhorter and Sunada approach is in a particular choice of the entry wetting-phase flux which allows the analytical implicit formula to be obtained. In Fučík et al. (2007) an improved version of this approach is presented which attempts to overcome the above-described difficulties. The improved method for resolution of the analytical formula works for any choice of entry-saturation values. However, it is shown that the entry flux profile allowing for the analytical treatment cannot be generalized.

In this article we therefore present use of the semi-analytical approach and comment on its output. We also consider the possibility of obtaining the solution to the transport problem based on the numerical solution of the advection-diffusion equation by means of the method of lines (Schiesser, 1991). We perform a series of qualitative and quantitative computations which show that our algorithm agrees with previously obtained results, and that we are able to deliver a more general class of numerical data which can serve as benchmarks for testing complex multidimensional models.

2. ONE-DIMENSIONAL TWO-PHASE FLOW BENCHMARK

2.1. Equations

In this section we present the transport problem with capillarity related to the two-phase flow in porous medium. We begin with a one-dimensional problem describing flow of two incompressible immiscible liquids through the porous medium where the non-wetting phase (indexed n) is displaced by the wetting liquid (water, indexed w) horizontally (therefore without the influence of gravity). In agreement with McWhorter and Sunada (1990), the below-described formulation by means of the fractional flow function allows a transport-type equation for saturation to be obtained which can be treated analytically. The Darcy law for the wetting and non-wetting phases has the form

$$q_{\mathrm{w}} = -\frac{k_{\mathrm{w}}}{\mu_{\mathrm{w}}}\frac{\partial p_{\mathrm{w}}}{\partial x}, \quad q_{\mathrm{n}} = -\frac{k_{\mathrm{n}}}{\mu_{\mathrm{n}}}\frac{\partial p_{\mathrm{n}}}{\partial x} \tag{1}$$

where k_{w}, k_{n}, μ_{w}, μ_{n}, p_{w}, and p_{n} are the effective permeabilities, viscosities, and pressures of corresponding phases. The total volumetric flux q_{t} consists of the wetting-phase part q_{w} and non-wetting-phase part q_{n}: $q_t = q_{\mathrm{w}} + q_{\mathrm{n}}$. The capillary relation

$$p_{\mathrm{c}} = p_{\mathrm{n}} - p_{\mathrm{w}} \tag{2}$$

with a given function $p_{\mathrm{c}} = p_{\mathrm{c}}(S_{\mathrm{w}})$ of the wetting-phase saturation S_{w} is used. Note that the non-wetting phase saturation S_{n} satisfies the condition $S_{\mathrm{n}} = 1 - S_{\mathrm{w}}$. Introducing the fractional flow and diffusivity functions,

$$f(S_{\mathrm{w}}) = \frac{k_{\mathrm{w}}(S_{\mathrm{w}})\,\mu_{\mathrm{n}}}{k_{\mathrm{w}}(S_{\mathrm{w}})\,\mu_{\mathrm{n}} + k_{\mathrm{n}}(S_{\mathrm{w}})\,\mu_{\mathrm{w}}}$$
$$D(S_{\mathrm{w}}) = -\frac{k_{\mathrm{n}}(S_{\mathrm{w}})}{\mu_{\mathrm{n}}} f(S_{\mathrm{w}}) \frac{dp_{\mathrm{c}}(S_{\mathrm{w}})}{dS_{\mathrm{w}}} \tag{3}$$

we have the expression for the wetting-phase flux

$$q_{\mathrm{w}} = f(S_{\mathrm{w}})q_{\mathrm{t}} - D(S_{\mathrm{w}})\frac{\partial S_{\mathrm{w}}}{\partial x} \tag{4}$$

Considering the porosity of the material, assuming constant density and no volumic source of mass, the mass balance has the following form,

$$\frac{\partial q_{\mathrm{w}}}{\partial x} + \Phi\frac{\partial S_{\mathrm{w}}}{\partial t} = 0 \tag{5}$$

where Φ is the porosity coefficient. The two-phase flow equation is obtained by substituting (4) into the mass balance

$$\Phi\frac{\partial S_{\mathrm{w}}}{\partial t} = -q_{\mathrm{t}}\frac{df(S_{\mathrm{w}})}{dS_{\mathrm{w}}}\frac{\partial S_{\mathrm{w}}}{\partial x} + \frac{\partial}{\partial x}\left[D(S_{\mathrm{w}})\frac{\partial S_{\mathrm{w}}}{\partial x}\right] \tag{6}$$

The Eq. (6) is accompanied by the initial condition for S_{w} and by corresponding boundary conditions for S_{w} at $x = 0$ and $x = +\infty$. Equation (6) is our main concern. We describe circumstances under which it can be solved analytically or numerically so that it can provide a simple one-dimensional benchmark data for the validation of more complex two-phase flow models, as has been done, e.g., in Mikyška et al. (2009). Our approach allows extension of the solution of Eq. (6), described originally in McWhorter and Sunada (1990), and improved in Fučík et al. (2007) to a family of time-dependent input fluxes $q_{\mathrm{t}} = q_{\mathrm{t}}(t)$, generalizing the use of this benchmark.

When capillary effects represented by the term

$$\frac{dp_{\mathrm{c}}(S_{\mathrm{w}})}{dS_{\mathrm{w}}} \tag{7}$$

in the diffusivity function are neglected, the term $D(S_{\mathrm{w}})$ in Eq. (6) vanishes and we obtain the Buckley–Leverett transport equation

$$\Phi\frac{\partial S_{\mathrm{w}}}{\partial t} = -q_{\mathrm{t}}\frac{df(S_{\mathrm{w}})}{dS_{\mathrm{w}}}\frac{\partial S_{\mathrm{w}}}{\partial x} \tag{8}$$

which also can be analytically solved as discussed, e.g., in Helmig (1997) or Fučík et al. (2007).

2.2. Analytical Solution

Usefulness of a benchmark problem consists in the relative simplicity of its solution. In this section we summarize the analytical treatment of Eq. (6), and in

the next section we describe the numerical treatment of it. A closed-form expression for the solution of Eq. (6) is presented in McWhorter and Sunada (1990), commented on in Chen et al. (1992), McWhorter and Sunada (1992), and improved in Fučík et al. (2007). A quasi-stationary solution of (6) under a very particular choice of the conditions can be found. We assume that

$$q_{\mathrm{w}}(t,0) = q_0(t) = Ag(t), \quad S_{\mathrm{w}}(t,+\infty) = S_{\mathrm{i}}$$
$$S_{\mathrm{w}}(0,x) = S_{\mathrm{i}} \tag{9}$$

where A and S_{i} are given constants. Then, a relationship between the constant A and the boundary condition $S_{\mathrm{w}}(t,0) = S_0$ exists under the circumstances discussed below. In McWhorter and Sunada (1990) and Fučík et al. (2007), it is shown that the function $g(t)$ has to have a particular form such that we are able to convert Eq. (6) into an equation independent of t,

$$g(t) = t^{-\frac{1}{2}} \tag{10}$$

even though it can be slightly generalized as in Fučík et al. (2007). The solution of (6) is hidden in the inverse formula

$$x(t, S_{\mathrm{w}}) = \frac{2A\left(1 - f\left(S_{\mathrm{i}}\right)R\right)}{\Phi g(t)} \frac{dF}{dS_{\mathrm{w}}}\left(S_{\mathrm{w}}\right) \tag{11}$$

where $R = 0$ for the countercurrent flow, and $R = 1$ for the unidirectional flow (for values of R between 0 and 1, see Fučík et al., 2008). The fractional flow function $F = F(S_{\mathrm{w}})$ is determined by the integral equation

$$F\left(S_{\mathrm{w}}\right) = 1 - \frac{\int_{S_{\mathrm{w}}}^{S_0} \frac{(s - S_{\mathrm{w}})D(s)}{F(s) - f_{\mathrm{n}}(s)} ds}{\int_{S_{\mathrm{i}}}^{S_0} \frac{(s - S_{\mathrm{i}})D(s)}{F(s) - f_{\mathrm{n}}(s)} ds} \tag{12}$$

with

$$f_{\mathrm{n}}\left(s\right) = R\frac{f\left(s\right) - f\left(S_{\mathrm{i}}\right)}{1 - f\left(S_{\mathrm{i}}\right)R} \tag{13}$$

Use of the analytical formula (12) is indirect, as it has the form of an implicit functional equation, from which $F\left(S_{\mathrm{w}}\right)$ has to be extracted. This can be done using the following iteration schemes.

First type of iteration scheme. A numerical iterative scheme described in McWhorter and Sunada (1990) has the following form:

$$F_{k+1}\left(S_{\mathrm{w}}\right) = 1 - \frac{\int_{S_{\mathrm{w}}}^{S_0} \frac{(s - S_{\mathrm{w}})D(s)}{F_k(s) - f_{\mathrm{n}}(s)} ds}{\int_{S_{\mathrm{i}}}^{S_0} \frac{(s - S_{\mathrm{i}})D(s)}{F_k(s) - f_{\mathrm{n}}(s)} ds} \tag{14}$$

According to McWhorter and Sunada (1990) and McWhorter and Sunada (1992), it is recommended to use $F_1\left(s\right) \equiv 1$ as the first iteration. In the case when S_0 satisfies $S_{\mathrm{i}} \leq S_0 < S_{\mathrm{m}}$ where $S_{\mathrm{m}} = 1 - S_{\mathrm{nr}}$, S_{nr} is the residual saturation of the non-wetting phase, discrete values of $F\left(S_{\mathrm{w}}\right)$ can be computed, and consequently, the constant$A$ is evaluated by the formula

$$A^2 = \frac{\Phi}{2\left[1 - f\left(S_{\mathrm{i}}\right)R\right]^2} \int_{S_{\mathrm{i}}}^{S_0} \frac{\left(s - S_{\mathrm{i}}\right)D\left(s\right)}{F\left(s\right) - f_{\mathrm{n}}\left(s\right)} ds \tag{15}$$

The main obstacle of this approach is the numerical behavior of the iteration scheme (14) for values $S_0 \to S_{\mathrm{m}}$, $R = 1$ when using real parameter values and material functions (see models 1 and 3 in Appendix A). Difficulties can be encountered when computing integrals in Eq. (14) numerically in some cases, namely because the values $F_k(s)$ and $f_{\mathrm{n}}(s)$ approached each other [see the denominator in the integrals of Eq. (14)]. This causes the iteration process to be unstable.

Second type of iteration scheme. The above-described facts led in Fučík et al. (2007) to a modification of the iteration method. Denoting the significant part of the integrand in Eq. (12) as

$$G\left(s\right) = \frac{D\left(s\right)}{F\left(s\right) - f_{\mathrm{n}}\left(s\right)} \tag{16}$$

allows Eq. (12) to be rewritten in a suitable way,

$$F(S_w) = f_n(S_w) + \frac{D(S_w)}{G(S_w)} = 1 - \frac{\int_{S_w}^{S_0} (s - S_w) G(s) ds}{\int_{S_i}^{S_0} (s - S_i) G(s) ds} \quad (17)$$

We then can use two variants of iterative schemes. The *variant A* is given by

$$G_{k+1}(S_w) = D(S_w) + G_k(S_w^*) \times \left(f_n(S_w) + \frac{\int_{S_w}^{S_0} (s - S_w) G_k(s) ds}{\int_{S_i}^{S_0} (s - S_i) G_k(s) ds} \right) \quad (18)$$

and the *variant B* is given by

$$G_{k+1}(S_w) = [D(S_w) + G_k(S_w) f_n(S_w)] \times \left(1 - \frac{\int_{S_w}^{S_0} (s - S_w) G_k(s) ds}{\int_{S_i}^{S_0} (s - S_i) G_k(s) ds} \right)^{-1} \quad (19)$$

According to Fučík et al. (2007), it is recommended to set

$$G_1(s) \equiv \frac{D}{1 - f_n(s)} \quad (20)$$

as the first iteration. The integrals in Eqs. (18) and (19) are evaluated numerically by means of the Newton–Cotes numerical integration formulae with the mesh size indicated in the figure captions. The schemes (18) and (19) exhibit convergence in all situations, except of values S_0 and R close to 1, as it is demonstrated in Figs. 1 and 2 where we have used the model 1 functions (see Appendix A for model description and for the particular values used). The iteration process is stopped when the difference between successive estimates of F is less or equal to 5×10^{-6}. The schemes given by Eqs. (18) and (19) extend the possibility of semianalytical treatment of of Eq. (6) in comparison to the scheme given by Eq. (14), as discussed in Fučík et al. (2007).

Figure 1 demonstrates that the solutions of Eq. (6) for $R = 0$ and $R = 1$ have similar shape for lower values of S_0 but they differ for values of S_0 close to S_m. This fact can be observed for all models used. However, for fixed S_0, similarity of saturation profiles for $R = 0$ and $R = 1$ can differ for different capillarity models, as they influence the relationship of diffusion and advection terms in a different way. In the case of S_0 being close to S_m, the scheme given by Eq. (14) exhibits instabilities as discussed in Fučík et al. (2007). They occur due to the sensitivity of Eq. (14) to the model functions and parameters, namely, in the case of real fluids (model 1). For model 2 used in McWhorter and Sunada (1990), but less related to real situations, they do not occur even if the value of S_0 is equal to S_m. Figure 2 compares the shape of solutions of Eq. (6) with capillary forces and of Eq. (8) without them. When the capillarity is much smaller than the advective term, the solution of (6) has a shape close to the Buckley–Leverett function.

The CPU usage of the benchmark implementation is given by the number of iterations (see Table 5 in Fučík et al., 2007). The iteration number increases when setting the values of S_0 and R close to 1. For details, see Table 1.

2.3. Numerical Solution of the Transport Equation

The above-described treatment of Eq. (6) led to the implicit formula (12) which had to be solved numerically anyway. This fact motivates us to propose another straight method of obtaining the solution of Eq. (6), so we derive a simple numerical scheme solving Eq. (6). It is based on the finite-difference method discretizing the spatial derivatives and subsequent solution of an ordinary differential equation system. In this case, we consider the following initial-boundary-value problem:

$$\Phi \frac{\partial S_w}{\partial t} = -q_t \frac{df(S_w)}{dS_w} \frac{\partial S_w}{\partial x} + \frac{\partial}{\partial x} \left(D(S_w) \frac{\partial S_w}{\partial x} \right)$$
$$S_w(t, 0) = S_0 \quad S_w(t, L) = S_i \quad (21)$$
$$S_w(0, x) = S_i$$

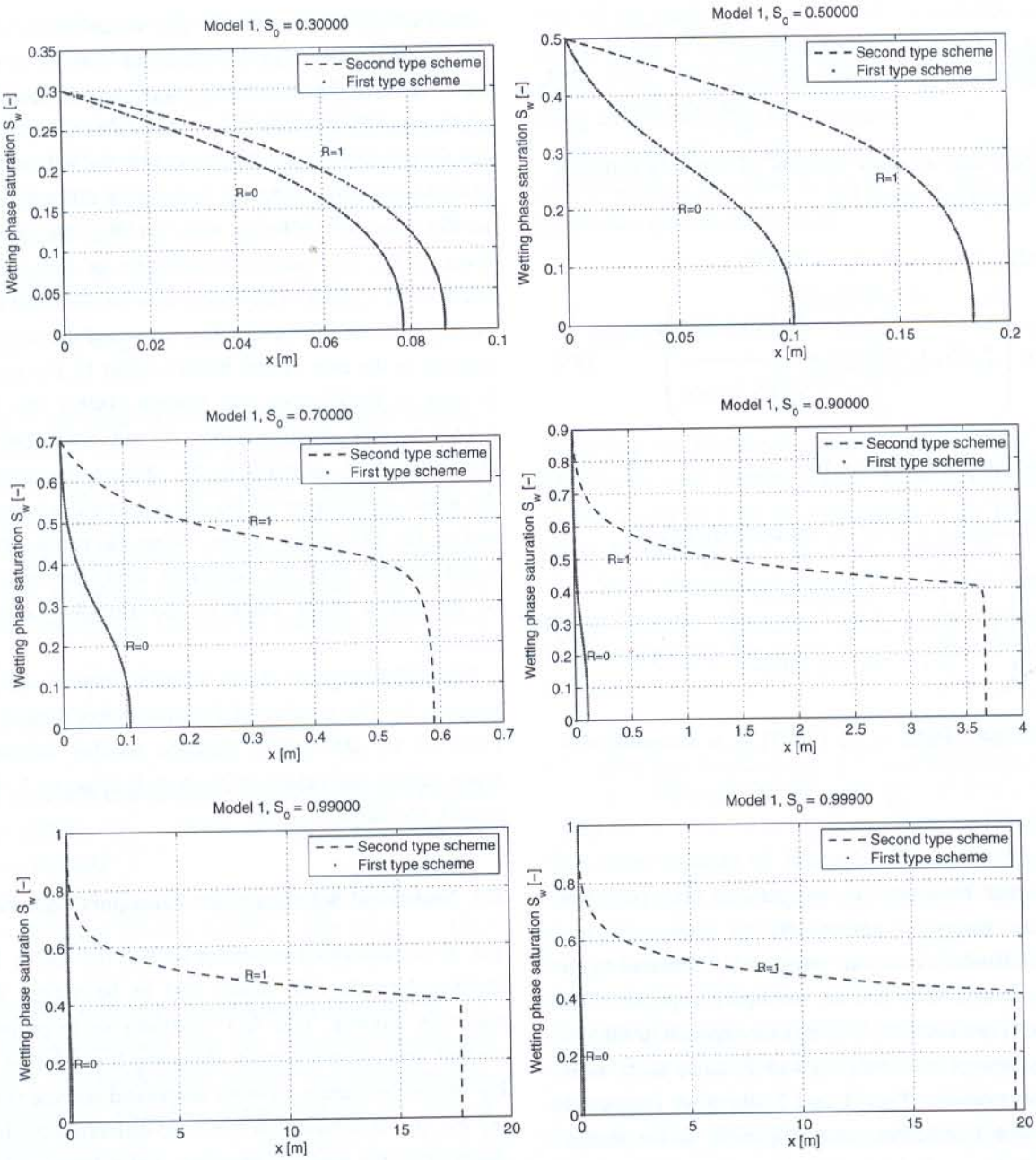

Figure 1. Graphs of the function $S_{\mathrm{w}} = S_{\mathrm{w}}(t,x)$ as a solution of Eq. (6) at time $t = 10,000s$ obtained by the schemes (14) (first type) and (19) (second type). The scheme (18) yields identical values as the scheme (19). Number of mesh nodes is 1000, and model 1 provides the capillarity and permeability properties

for $t \in [0,T]$ and $x \in (0,L)$, where L is length of the spatial interval and T is the final time considered. We discretize (6) on a uniform spatial grid of $M+1$ nodes with the mesh size $h = L/M$ covering the interval $(0,L)$. We denote nodal values of the function S_{w} as $\{S_{\mathrm{w}j}(t) \,|\, j = 0,\ldots,M\}$ [i.e., $S_{\mathrm{w}j}(t) = S_{\mathrm{w}}(t,jh)$].

Table 1

Values of CPU time used in analytical computation by Eq. (18) with M =1000 spatial nodes and iteration tolerance $\varepsilon = 10^{-10}$ to get the selected time level directly, and in numerical computation with M =100, 200 spatial nodes and time step $\tau = 0.1$, 0.01 to get all successive time levels prior to the selected time. The entry flux is given by $g(t) = t^{-1/2}$. For computations, the processor Core 2 6600 with the CPU clock 2.40GHz and the cache 4096 kB were used

S_0	R	**Analytical solution**	**Numerical solution**	
		M = 1000, $\varepsilon = 10^{-10}$	$M = 100$, $\tau = 0.1$	$M = 400$, $\tau = 0.01$
0.5	0	20 ms	1 min, 29 s, 110 ms	13 min, 17 s, 270 ms
	1	20 ms	1 min, 27 s, 770 ms	12 min, 38 s, 320 ms
0.7	0	20 ms	1 min, 33 s, 930 ms	12 min, 47 s, 290 ms
	1	30 ms	1 min, 36 s, 480 ms	14 min, 18 s, 620 ms
0.9	0	30 ms	1 min, 30 s, 30 ms	13 min, 3 s, 440 ms
	1	140 ms	1 min, 42 s, 880 ms	15 min, 9 s, 140 ms
0.99	0	20 ms	1 min, 30 s, 350 ms	13 min, 5 s, 560 ms
	1	4 s 0 ms	1 min, 37 s, 790 ms	14 min, 26 s, 750 ms

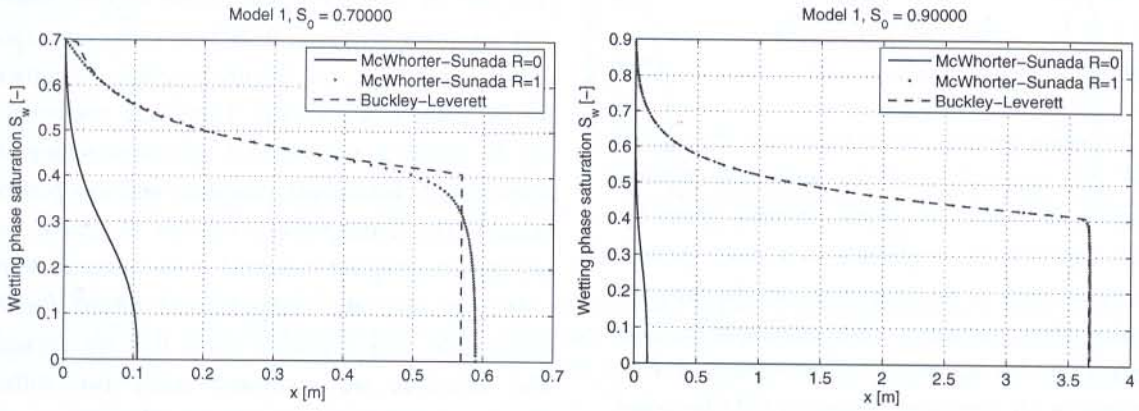

Figure 2. Graphs of the function $S_w = S_w(t, x)$ as a solution of Eq. (6) at time $t = 10,000s$ obtained by the schemes (14) (first type) and (19) (second type). The scheme (18) yields identical values as the scheme (19). Number of mesh nodes is 1000, and model 1 provides the capillarity and permeability properties

The second-order differential operator is discretized by the central-difference formula with second-order accuracy,

$$\left.\frac{\partial}{\partial x}\left(D(S_w)\frac{\partial S_w}{\partial x}\right)\right|_j \approx \left[D\left(\frac{S_{w,j+1}+S_{wj}}{2}\right)\times(S_{w,j+1}-S_{wj}) - D\left(\frac{S_{wj}+S_{w,j-1}}{2}\right)\times(S_{wj}-S_{w,j-1})\right]/[h^2] \quad (22)$$

and the advection term is discretized by means of the upwind approach (see LeVeque, 1990) with first-order accuracy

$$\left.\frac{df(S_w)}{dS_w}\,\frac{\partial S_w}{\partial x}\right|_j \approx \frac{f(S_{wj}) - f(S_{wj-1})}{h} \quad (23)$$

The solution $\{S_{wj}(t)\,|j = 0, \ldots, M\}$ is found from the semidiscrete scheme representing a system of $M - 1$ ordinary differential equations in the form

$$\Phi \frac{dS_{wj}}{dt} = -q_t(t)\frac{f(S_{wj}) - f(S_{wj-1})}{h} \quad (24)$$
$$+ \left[D\left(\frac{S_{w,j+1} + S_{wj}}{2}\right)(S_{w,j+1} - S_{wj}) \right.$$
$$\left. - D\left(\frac{S_{wj} + S_{w,j-1}}{2}\right)(S_{wj} - S_{w,j-1}) \right] / [h^2]$$
$$\text{for } j = 1, \cdots, M-1, \text{ with } S_{w0}(t) = S_0$$
$$S_{wM}(t) = S_i \text{ and } S_{wj}(0) = S_i,\ j = 1, \ldots, M-1$$

System (24) is numerically resolved by means of the Runge–Kutta fourth-order method with a fixed time step $\tau > 0$ (see Schiesser, 1991).

Similarly, we can treat the Buckley–Leverett Eq. (8) proposing the semidiscrete scheme

$$\Phi \frac{dS_{wj}}{dt} + q_t(t)\frac{f(S_{wj}) - f(S_{wj-1})}{h} = 0$$
$$\text{for } j = 1, \cdots, M, \text{ with } u_0(t) = S_0$$
$$\text{and } S_{wj}(0) = S_i,\ j = 1, \ldots, M \quad (25)$$

In the following section, we demonstrate the agreement of this approach with the analytical method described in section 2. However, schemes given by Eqs. (24) and (25) are applicable in a more general framework – there is no restriction on the function $q_t(t)$ other than continuity with respect to t. The CPU usage of this approach is low (order of tens of seconds) in all situations. Equation (21) becomes close to hyperbolic for S_0 and R close to 1. This is compensated by the upwind character of scheme (24) (for details, see Table 1). Computational complexity of formulas in capillary and permeability models can slightly increase the CPU time, as they are used by the multistage time solver treating Eq. (24).

3. COMPUTATIONAL STUDIES

3.1. Comparing Analytical and Numerical Approaches

In Figs. 1 and 2 we used artificial test values and material dependencies for the sake of comparison of our results with those of McWhorter and Sunada (1990). In this section we demonstrate the reliability of our analytical (18)/(19) and numerical (24) approaches using coefficients and dependencies describing real medium and real non-wetting phase (the so-called NAPL—nonaqueous phase liquid—see Appendix A for particular values) together with a real capillarity model. Figure 3 shows how the two approaches agree. Each graph contains both the concurrent and countercurrent flow profiles. The value of A is given by the choice of the parameters S_0 and R and by formula (15). It follows that $A = 10^{-3}$.

3.2. Generalization of the Entry Flux

The algorithm (24) solving the problem (21) is applicable for any continuously time-dependent entry-flux profile $q_0(t) = Ag(t)$. Analogous to the previous case, we set $A = 10^{-3}$ and choose various functions $g(t)$ satisfying $g(0) = 1$. Results of such computations are shown in Figs. 4–7. Figure 8 contains comparison for the entry flux Eq. (10). They were computed using the model 1 and model 3 parameter settings (see Appendix A for model functions and for particular values). The corresponding number of spatial nodes and the time step are indicated in the figure captions.

In Figs. 4–8 the computational results for two-phase flow with a general entry flux are presented. The solutions are compared using two different choices of numerical parameters. The scheme given by Eq. (24) obeys the usual stability condition for explicit schemes $(D_{max}/\Phi)(\tau/h^2) \leq 1/2$, where D_{max} is the upper bound for values of the function $D(S_w)$ in formula (3). From the figures it can be seen that the numerical solution converges to the semianalytical one, even in places where it is steep, that is, where it has a large gradient. Obviously, this requires use of enough spatial grid points.

The analytical (18)/(19) and numerical (24) approaches are also compared with respect to the computational efficiency. Table 1 summarizes the CPU times in a given environment necessary to obtain the presented results. Computational complexity of the schemes given by Eqs. (18)/(19) increases for values S_0 and R approaching 1. The indicated time is

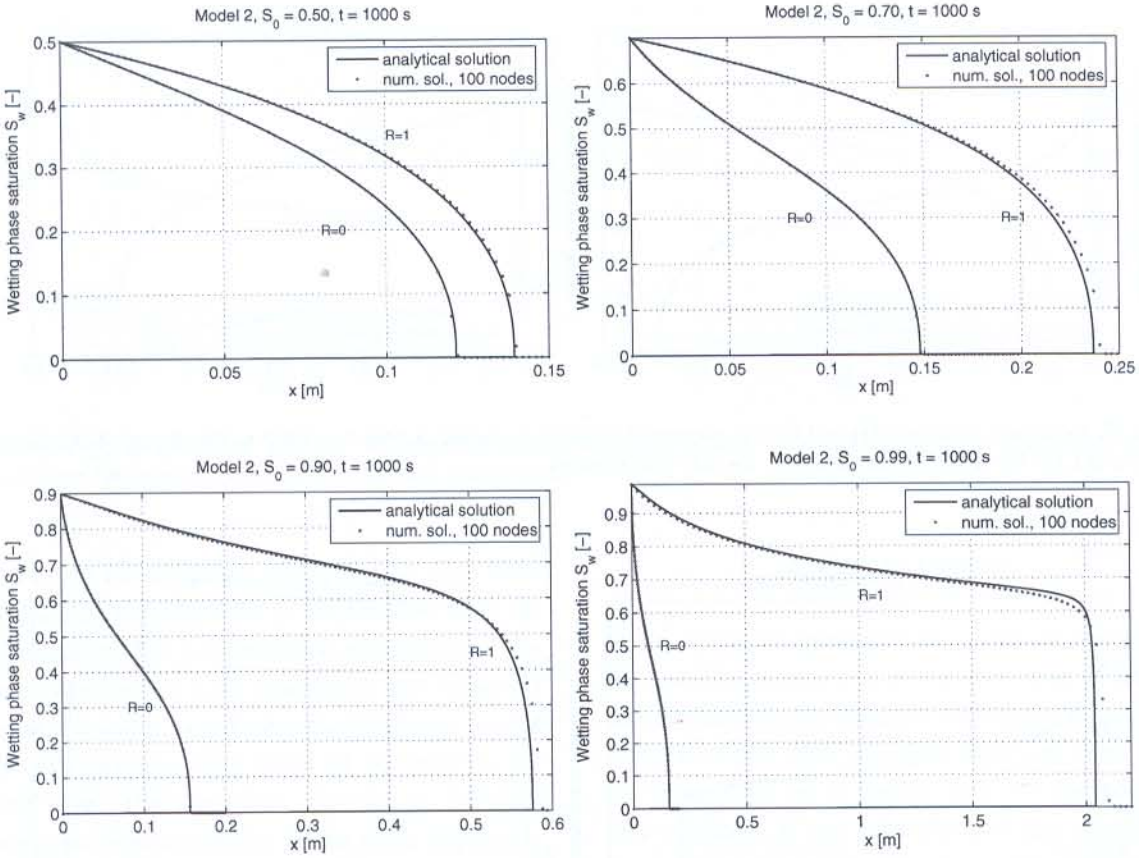

Figure 3. Results using the model 2 equations (see Appendix A), time t = 1000 s. The algorithm (18)/(19) is used to obtain the analytical solution using 1000 spatial nodes. Each numerical solution is dependent on the analytical solution through the value of the parameter A. Numerical results were obtained using a grid of 100 nodes, with the Runge–Kutta time step 0.1 for (24)

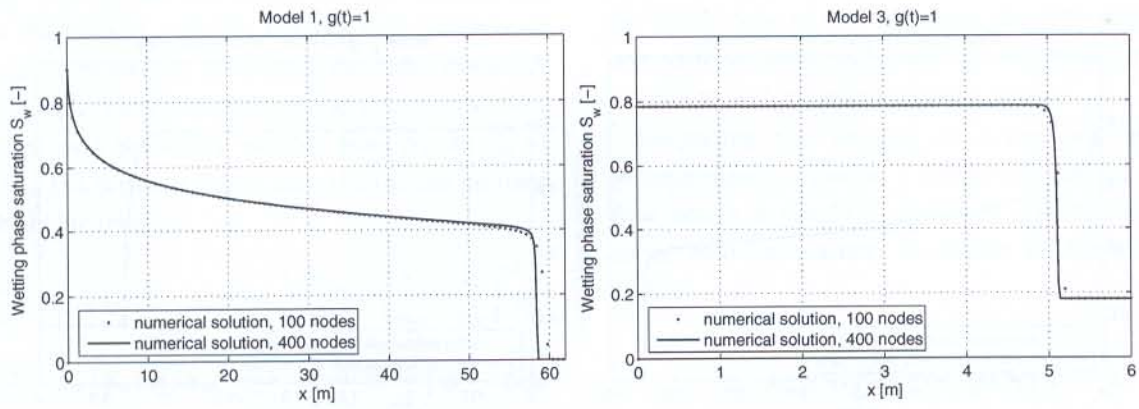

Figure 4. Input flux function $g(t) = 1$, numerical solution evaluated at time t = 1000 s. The Runge–Kutta time step for (24) is 0.1 for 100 spatial nodes and 0.01 for 400 spatial nodes

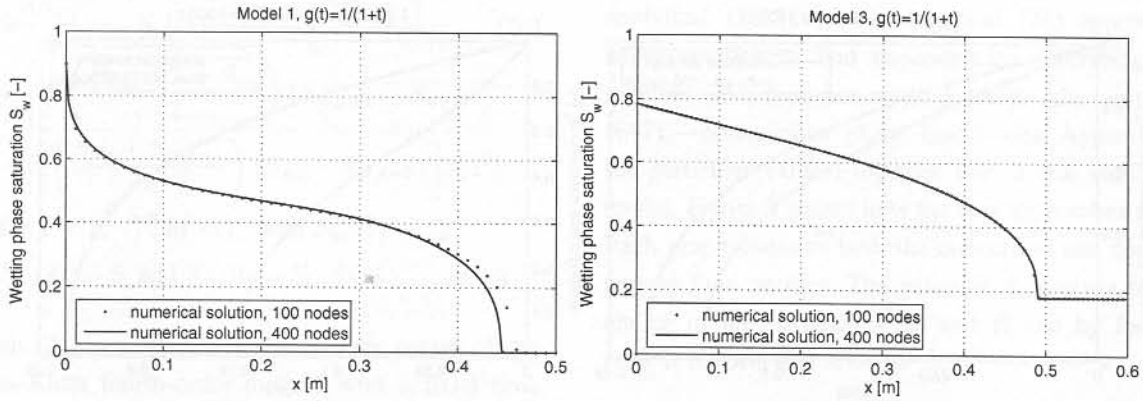

Figure 5. Input flux function $g(t) = 1/1 + t$, numerical solution evaluated at time t = 1000 s. The Runge–Kutta time step for (24) is 0.1 for 100 spatial nodes and 0.01 for 400 spatial nodes

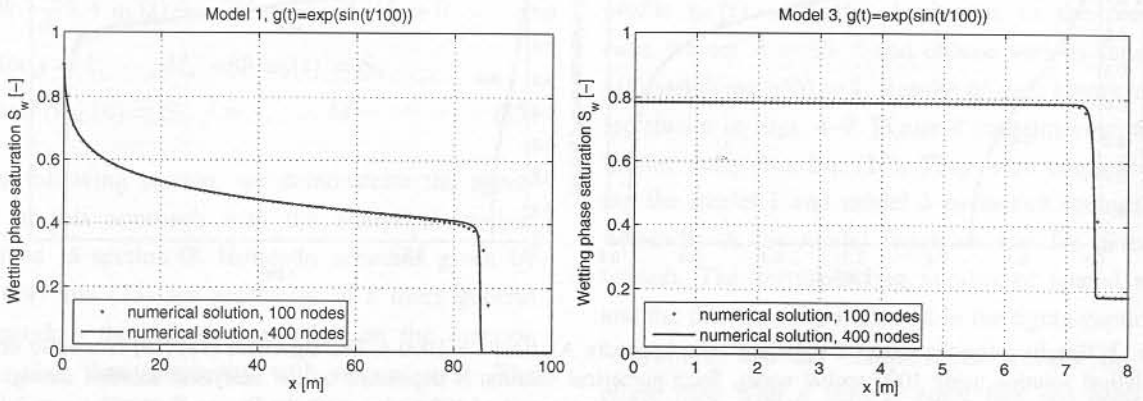

Figure 6. Input flux function $g(t) = \exp(\sin \frac{t}{100})$, numerical solution evaluated at time t = 1000 s. The Runge–Kutta time step for (24) is 0.1 for 100 spatial nodes and 0.01 for 400 spatial nodes

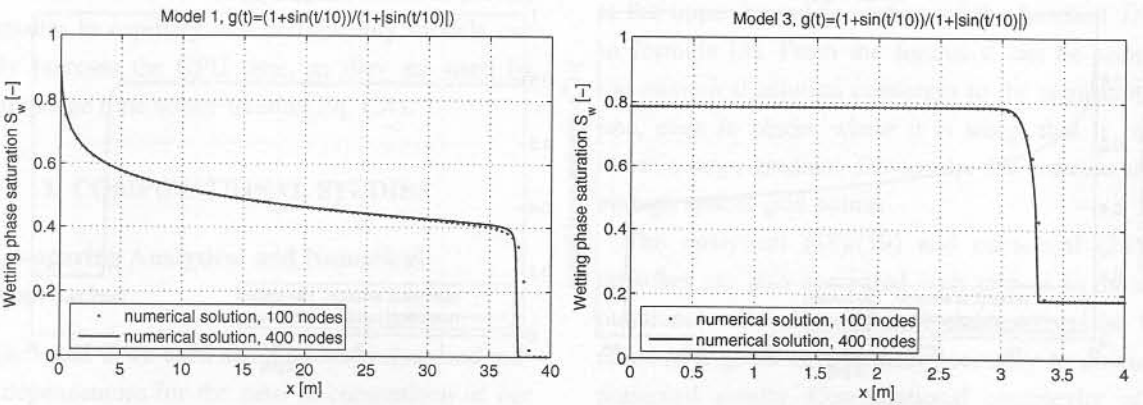

Figure 7. Input flux function $g(t) = \frac{1+\sin(t/10)}{1+|\sin(t/10)|}$, numerical solution evaluated at time t = 1000 s. The Runge–Kutta time step for (24) is 0.1 for 100 spatial nodes and 0.01 for 400 spatial nodes

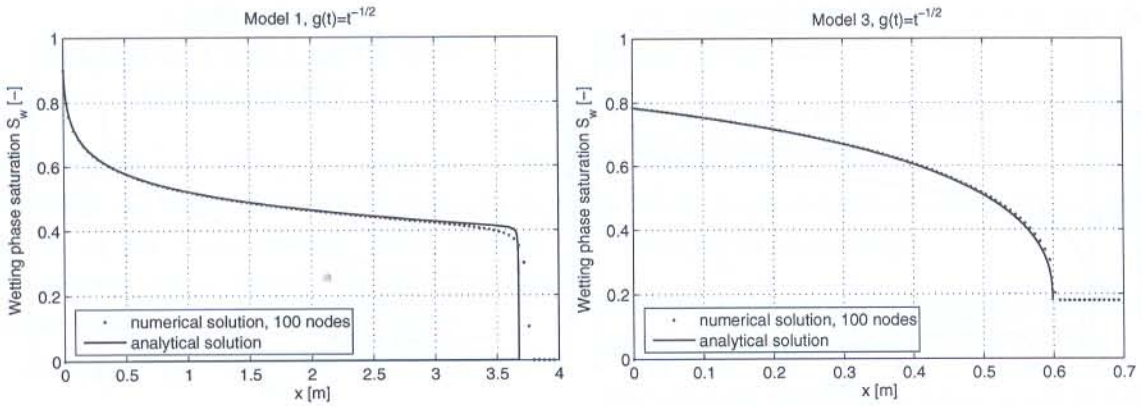

Figure 8. Input flux function $g(t) = t^{-\frac{1}{2}}$, numerical solution evaluated at time t = 1000 s. The Runge–Kutta time step for (24) is 0.1 for 100 spatial nodes and 0.01 for 400 spatial nodes

needed to get the stationary profile $F = F(S_w)$ from which the selected time level of the function S_w is directly obtained. The computational complexity of the scheme given by Eq. (24) depends on the numerical parameters h and τ. It indicates the CPU time needed to get all successive time levels of S_w prior to the selected time. The numerical approach is therefore slightly more time demanding (under given implementation) but it allows a general class of entry fluxes to be treated.

3.3. Secondary Variables

Both the semianalytical and the numerical approaches to Eq. (6) provide the values of the function S_w as of the primary variable. For practical purposes, it may be convenient to have other quantities available. For example, the non-wetting phase saturation is then obtained as a secondary variable from S_w as $S_n = 1 - S_w$. For pressure drops, Eqs. (1)–(4) can be used to obtain the relations

$$\frac{\partial p_w}{\partial x} = (f_w(S_w) - 1)\, p_c'(S_w) \frac{\partial S_w}{\partial x} - \left(\frac{k_w}{\mu_w} + \frac{k_n}{\mu_n}\right)^{-1} q_t$$
$$\frac{\partial p_n}{\partial x} = f_w(S_w)\, p_c'(S_w) \frac{\partial S_w}{\partial x} - \left(\frac{k_w}{\mu_w} + \frac{k_n}{\mu_n}\right)^{-1} q_t \qquad (26)$$

which use the derivative $\partial S_w/\partial x$. Examples of profiles for these quantities are presented in Fig. 9.

4. CONCLUSIONS

In the article we presented two types of benchmarks for one-dimensional two-phase flow. One of them is the semianalytically obtained wetting-phase saturation solution of the flow equation. This was done under the assumption of a special form of the boundary flux condition. If any other form of this condition is required, the second benchmark can be used which is based on the numerical solution of the flow equation by means of the finite-difference method of lines. The two benchmarks were compared in situations when it was possible. The semianalytical approach provides accurate values of the wetting-phase saturation but becomes computationally more expensive for values S_0 and R close to to 1. However, the fully numerical approach can work with rather general boundary flux conditions and is computationally efficient.

Respecting the demands of testing with respect to heterogeneous media, a benchmark for two-phase flow across a simple discontinuity can be designed using both approaches, as shown in Fučík et al. (2008).

ACKNOWLEDGMENTS

The authors were partly supported by the project "Applied Mathematics in Technical and Physical Sci-

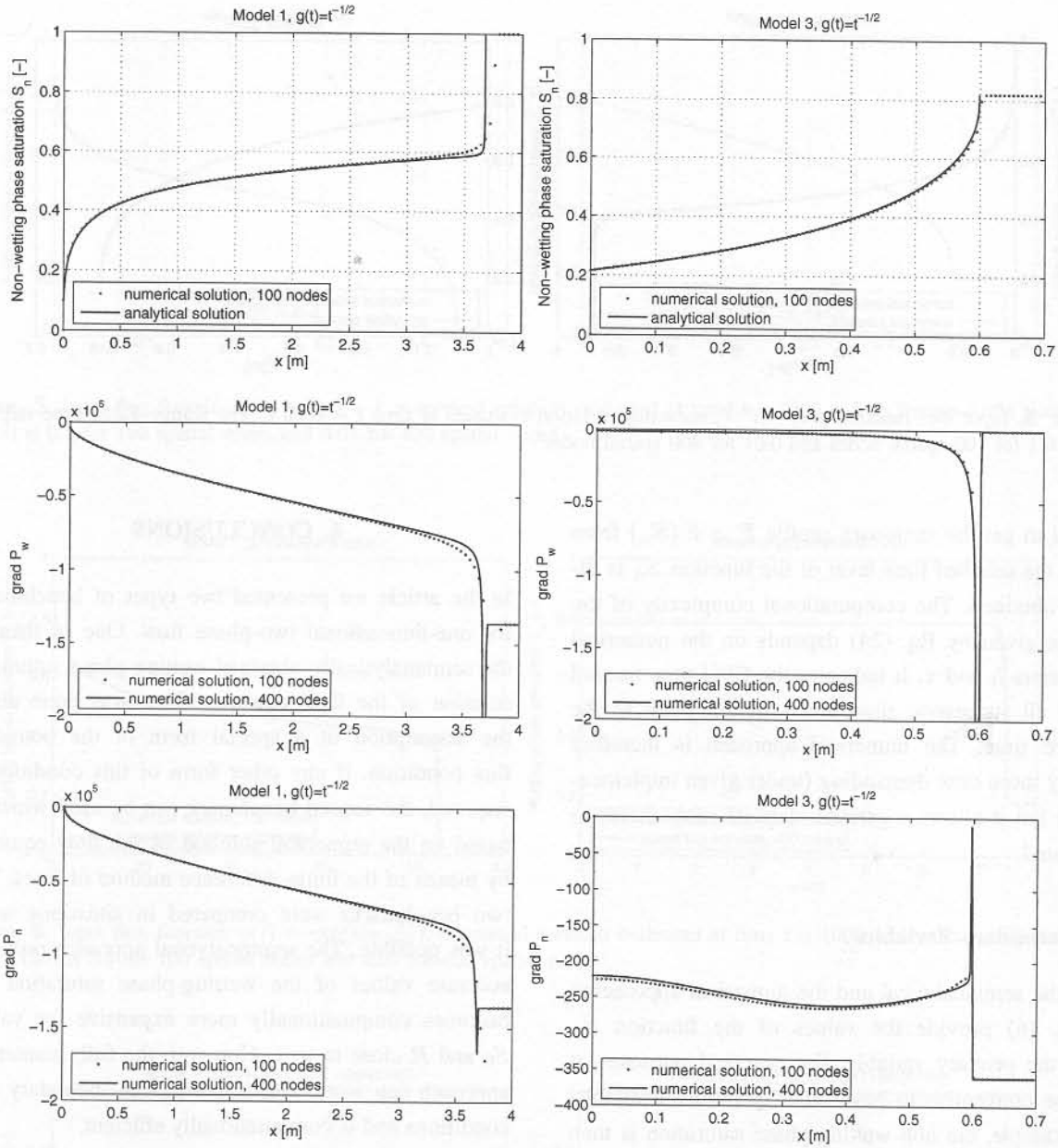

Figure 9. Example of secondary-variable profiles for the input flux function $g(t) = t^{-\frac{1}{2}}$, numerical solution evaluated at time t = 1000 s. The Runge–Kutta time step for (24) is 0.1 for 100 spatial nodes and 0.01 for 400 spatial nodes. Setting corresponds to Fig. 8

ences," MSM 6840770010, by the project "Environmental Modelling," KONTAKT ME878, and by the project "Jindřich-Nečas Center for Mathematical Modelling," LC06052, all of the Ministry of Education of the Czech Republic, and by the National Science Foundation through Award 0222286 (CMG RESEARCH: "Numerical and Experimental Validation of Stochastic Upscaling for Subsurface Contamination Problems Involving Multi-Phase Volatile Chlorinated Solvents").

APPENDIX A
MODELS OF CAPILLARITY AND PERMEABILITY

Throughout the article we have used models described in McWhorter and Sunada (1990). This choice allows comparison of our results with the results obtained in this reference and in related references. The Van Genuchten capillarity model reads as

$$p_c\left(S_w\right) = p_0\left(S_w^{-\frac{1}{m}} - 1\right)^{1-m}, \text{ for } p_c > 0 \quad (27)$$

or the Brooks–Corey capillarity model (Helmig, 1997)

$$p_c\left(S_w\right) = p_0 S_w^{-\frac{1}{\lambda}}, \text{ for } p_c \geq p_0 \quad (28)$$

The permeability functions were described by the Mualem model (Mualem, 1976)

$$\begin{aligned} k_w\left(S_e\right) &= k_0 S_e^{\frac{1}{2}}\left(1 - \left(1 - S_e^{\frac{1}{m}}\right)^m\right)^2 \\ k_n\left(S_e\right) &= k_0\left(1 - S_e\right)^{\frac{1}{3}}\left(1 - S_e^{\frac{1}{m}}\right)^{2m} \end{aligned} \quad (29)$$

or by the Parker model (Parker et al., 1987)

$$\begin{aligned} k_w\left(S_e\right) &= k_0 S_e^{\frac{1}{2}}\left(1 - \left(1 - S_e^{\frac{1}{m}}\right)^m\right)^2 \\ k_n\left(S_e\right) &= k_0\left(1 - S_e\right)^{\frac{1}{2}}\left(1 - S_e^{\frac{1}{m}}\right)^{2m} \end{aligned} \quad (30)$$

The Burdine model for permeability (as in Helmig, 1997) reads as

$$\begin{aligned} k_w\left(S_e\right) &= k_0 S_e^{\frac{2+3\lambda}{\lambda}} \\ k_n\left(S_e\right) &= k_0\left(1 - S_e\right)^2\left(1 - S_e^{\frac{2+\lambda}{\lambda}}\right) \end{aligned} \quad (31)$$

The above formulas depend on the effective saturation S_e defined by

$$S_e(S_w) = \frac{S_w - S_{wr}}{1 - S_{wr} - S_{nr}} = \frac{S_w - S_{wr}}{S_m - S_{nr}} \quad (32)$$

where S_{wr} and S_{nr} are residual saturations of respective phases.

We couple the above given formulas into the following configurations:

- Model 1 considering the formula (28) for capillarity and (31) for permeability.
- Model 2 considering the formula (27) for capillarity and (30) for permeability.
- Model 3 considering the formula (27) for capillarity and (29) for permeability.

We have used the parameter values shown in Table A–1. The setting for models 1 and 2 corresponds to the values selected in such a way that the ratio μ_w/μ_n is larger and allows testing the behavior of the model in extreme situations. Model 3 uses the parameters of real liquids [w = water, n = NAPL liquid 1,2 DCE, see Grant and Gerhard (2004), p. 62].

REFERENCES

Beneš, M., Illangasekare, T. H., and Mikyška, J., *On the Numerical Treatment of Sharp Texture Transitions in Two-Phase Flow*, In Beneš, M., Kimura, M., and Nakaki, T., Eds., *Proc. of Czech Japanese Seminar in Applied Mathematics 2005*, COE Lecture Notes Vol. 3, Faculty of Mathematics, Kyushu University Fukuoka, ISSN 1881-4042, pp. 106–116, 2006.

Chen, Z. X., Bodvarsson, G. S., and Witherspoon, P. A., Comment on "Exact Integral Solutions for Two-Phase Flow," by McWhorter, D. B. and Sunada, D. K., *Wat. Resour. Res.*, vol. **28**, pp. 1477–1478, 1992.

Fučík, R., Illangasekare, T. H., and Mikyška, J., Evaluation of Saturation-Dependent Flux on Two-Phase Flow Using Generalized Semi-Analytic Solution, in Beneš, M. et al., Editors, *Proc. of the Czech Japanese Seminar in Applied Mathematics*, Prague, Faculty of Nuclear Sciences and Physical Engineering, Czech Technical University in Prague, pp. 23–35, 2005.

Fučík, R., Mikyška, J., Illangasekare, T. H., and Beneš, M., Improvement to semi-analytical solution for validation of numerical models of two-phase porous-media flow, *Vadose Zone J.*, vol. **6**, pp. 93–104, ISSN 1539-1663, 2007.

Fučík, R., Mikyška, J., Illangasekare, T. H., and Beneš, M., Semi-Analytical Solution for Two-Phase

Table A–1
Values used as a test model in numerical and analytical computation

	Model 1	Model 2	Model 3
Respective model parameters	$\lambda = 2$ $p_0 = 1000$ Pa	$m = 0.5$ $p_0 = 1000$ Pa	$m = 0.7778$ $p_0 = 3000$ Pa
Averaged porosity [-]	$\phi = 0.3$	$\phi = 0.3$	$\phi = 0.3$
Soil permeability [m^2]	$k_0 = 10^{-10}$	$k_0 = 10^{-10}$	$k_0 = 10^{-10}$
Dynamic viscosity [kg m^{-1} s^{-1}]	$\mu_w = 0.050$ $\mu_n = 0.001$	$\mu_w = 0.050$ $\mu_n = 0.001$	$\mu_w = 0.001$ $\mu_n = 0.00088$
Residual saturation [-]	$S_{wr} = 0$ $S_{nr} = 0$	$S_{wr} = 0$ $S_{nr} = 0$	$S_{wr} = 0.180$ $S_{nr} = 0.148$
Initial saturation [-]	$S_i = 0$	$S_i = 0$	$S_i = 0.180$
Maximal saturation [-]	$S_m = 1$	$S_m = 1$	$S_m = 0.852$

Flow in Porous Media with a Discontinuity, *Vadose Zone J.*, vol. **7**, pp. 1001–1007, ISSN 1539-1663, 2008.

Grant, G. P., and Gerhard, J. I., Sensitivity of Predicted DNAPL Source Zone Longevity to Mass Transfer Correlation Model, in Young, R. N. and Thomas, H. R., Eds., *Geoenvironmental Engineering: Integrated Management of Groundwater and Contaminated Land,* London: Telford Publishing, pp. 59–67, 2004.

Helmig, R., *Multiphase Flow and Transport Processes in the Subsurface, A Contribution to the Modelling of Hydrosystems*, Springer: New York, 1997.

LeVeque, R., *Numerical Methods for Conservation Laws, ETH Lectures in Mathematics Series,* Basel: Birkhäuser Verlag, 1990.

McWhorter, D. B., and Sunada, D. K., Exact Integral Solutions for Two-Phase Flow, *Water Resour.,* vol. **26**, pp. 399–413, 1990.

McWhorter, D. B., and Sunada, D. K., Reply, *Water Resour. Res.*, vol. **28**, p. 1479, 1992.

Mikyška, J., Beneš, M., Turner, A., and Illangasekare, T. H., Development and Validation of a Multiphase Flow Model for Applications in NAPL Behavior in Highly Heterogeneous Aquifer Formations, in Kovar, K. et al., Eds., *Proc. on FEM MODFLOW and More*, Prague: Charles University, pp. 215–218, 2004.

Mikyška, J., and Illangasekare, T. H., Application of a Multiphase Flow Model for Simulations of NAPL Behavior at Inclined Material Interfaces, in Beneš, M., et al., Eds., *Proc. of the Czech Japanese Seminar in Applied Mathematics*, Prague, Faculty of Nuclear Sciences and Physical Engineering, Czech Technical University in Prague, pp. 11–127, 2005.

Mikyška, J., Beneš, M., and Illangasekare, T. H., Numerical Investigation of NAPL Behavior at Heterogeneous Sand Layers Using VODA Multiphase Flow Code, *J. Porous Media*, vol. **12**, 685–694, 2009.

Mualem, Y., A New Model for Predicting the Hydraulic Conductivity of Unsaturated Porous Media, *Water Resour. Res.,* vol. **12**, pp. 513–522, 1976.

Parker, J. C., Lenhard, R. J., and Kuppusamy, T., A Parametric Model for Constitutive Properties Governing Multiphase Flow in Porous Media, *Water Resour. Res.*, vol. **23**, pp. 618–624, 1987.

Schiesser, W. E., *The Numerical Method of Lines*, New York: Academic Press, 1991.